Decomposition and removal of hydrazine by Mn/MgAl-layered double hydroxides

Mahmoud M. Kamel[a,*], Mosaed S. Alhumaimess[a], Mohammad H. Alotaibi[b], Ibrahim H. Alsohaimi[a], Hassan M.A. Hassan[a,c], Hamed M. Alshammari[d], Obaid F. Aldosari[e,f]

[a]*Department of Chemistry, College of Science, Jouf University, P.O. Box: 2014, Sakaka, Kingdom of Saudi Arabia, Tel. +966 537106764; emails: mmkamel@ju.edu.sa (M.M. Kamel), mosaed@ju.edu.sa (M.S. Alhumaimess), ehalshaimi@ju.edu.sa (I.H. Alsohaimi), hmahmed@ju.edu.sa (H.M.A. Hassan)*
[b]*National Center of Petrochemicals Technology, King Abdulaziz City for Science and Technology, P.O. Box: 6089, 11442 Riyadh, Saudi Arabia, email: mhhalotaibi@kacst.edu.sa (M.H. Alotaibi)*
[c]*Department of Chemistry, Faculty of Science, Suez University, Suez, Egypt*
[d]*Chemistry Department, Faculty of Science, Ha'il University, P.O. Box: 2440, Ha'il, Saudi Arabia, email: hd1398@hotmail.com (H.M. Alshammari)*
[e]*Department of Chemistry, College of Science and Human Studies at Hautat Sudair, Majmaah University, P.O. Box: 66, 11952 Majmaah, Saudi Arabia, email: obaid987@gmail.com (O.F. Aldosari)*
[f]*Chemistry Department, College of Science and Humanities, Prince Sattam bin Abdulaziz University, P.O. Box: 83, 11942 Alkharj, Saudi Arabia*

ABSTRACT

The layered double hydroxide (MgAl-LDH) was modified by manganese for obtaining Mn/MgAl-LDH. The obtained material was characterized by inductively coupled plasma, X-ray powder diffraction, Fourier-transform infrared spectroscopy, scanning electron microscopy and X-ray photoelectron spectroscopy. The as-synthesized Mn/MgAl-LDH was investigated for the decomposition and removal of hydrazine in a batch system. Factors affecting the decomposition and removal of hydrazine such as pH, time, initial hydrazine concentration and temperature were optimized. At the optimal pH 8, Mn/MgAl-LDH dose (100 mg), time of 90 min and temperature of 293 K, the hydrazine decomposition and removal percentage was 100% for initial concentrations of 5, 10 and 15 mg L^{-1}. Where, the pure MgAl-LDH showed 14% removal at 90 min for 10 mg L^{-1} of hydrazine compared to Mn/MgAl-LDH. The decomposition of hydrazine increased when the temperature was increased from 293 to 318 K and the time of complete decomposition reduced from 90 to 45 min, respectively. The decomposition process of hydrazine on Mn/MgAl-LDH depended on the formed ions of manganese(II) and (III) as well as Mn$_3$O$_4$ on the surface. The existence of Mn^{3+} as a strong oxidant could decompose hydrazine to nitrogen and hydrogen. The catalytic decomposition of hydrazine was best followed by the first-order rate law and the calculated E_a value was found to be 24.841 kJ mol^{-1}. The simple methodology regarding the material preparation and the method used as well as its effectiveness may provide a promising future for the decomposition and removal of hydrazine.

Keywords: Layered double hydroxide (LDH); Manganese; Hydrazine; Decomposition; Removal

* Corresponding author.

1. Introduction

Hydrazine (N_2H_4) is an inorganic compound that has been involved in many important applications such as medicines, pesticides, plastic chemicals, rocket fuel, oxygen scavenger in boilers and catalysis [1]. Hydrazine is highly soluble in water and it may be percolated to water sources and soil causing pollution. Hydrazine pollution is hazardous for humans leading to serious health problems to the skin, lungs, kidney, liver and central nervous system [1–3]. Hence, mentoring and the effective removal of its releasing to the environment are insistently requested. Additionally, the high alkalinity of hydrazine aqueous solutions (pH ≥ 12) and its explosive nature make its remedy from aqueous solutions a challenge and great concern. Several studies have been focused on the decomposition of hydrazine based on the catalytic oxidation process using various oxidizing agents [4–9]. Hydrazine can be degraded in two ways to give N_2, H_2 and NH_3 (Eqs. (1) and (2)) [4].

Complete decomposition:

$$N_2H_{4(l)} \rightarrow N_{2(g)} + 2H_{2(g)} \tag{1}$$

Incomplete decomposition:

$$N_2H_{4(l)} \rightarrow 4NH_{3(g)} + N_{2(g)} \tag{2}$$

Besides trails for hydrazine decomposition in presence of catalysts [4–9], many efforts have been made to treat the seriousness of hydrazine contamination. Several methods have been applied such as: membrane separation techniques [10], ultrasonic irradiation [2], sonochemical decomposition [11], adsorption [12], and biodegradation [13]. Recently, some new materials have been developed and investigated for hydrazine removal and decomposition [3,14–16]. Layered double hydroxides (LDHs) belong to a group of 'non-silicate oxides and hydroxides' materials and they are also referred to as hydrotalcite-like compounds [17]. Their general formula can be presented as $[M^{2+}_{1-x}·M^{3+}_x(OH)_2]^{x+}[A^{n-}_{x/n}·yH_2O]^{x-}$ where M^{2+} and M^{3+} are divalent and trivalent metal ions, A^{n-} is an n^- valent anion and x may range between 0.20 and 0.33 [18]. The basic feature of such compounds is isomorphous replacing a portion of the divalent ions by trivalent ones resulting in positively-charged sheets on the layers [17]. LDHs have notable properties; they are characterized by structural stability due to their better crystallinity. They exhibit a high external surface area as well as the internal surface that can offer good binding sites for each singular hydroxide sheet. Generally, LDHs can be used in a wide range of applications such as photocatalysis [19,20] and adsorption of heavy metals from aqueous solutions [21–25]. Among the most widely applied hydrotalcite compounds, the MgAl-LDHs are non-toxic and cheap [18,26,27]. The MgAl-LDH and other LDHs can be easily synthesized using diverse methods [17,28]. Recently, there have been various studies including the design of MgAl-LDHs with various compositions according to the intended applications. Several intercalated MgAl-LDHs by different compounds have exhibited good environmental applications [18,29,30]. Manganese is an important element that has been involved in several biological systems and it is a basic factor in photosynthesis reactions [31].

It exhibits many oxidation states (+2, +3, +4 and +7) and forms different oxides and compounds. Manganese oxides have been applied in catalysis and electrochemistry [32]. LDHs containing manganese species have been utilized as oxidizing catalysts in many industrial processes and environmental treatments [31,33,34]. In this study, we intended to find out new material for removing hydrazine. The MgAl double hydroxides were our concern due to their characteristic properties. Hence, the study initially involved the preparation of the MgAl-LDHs which were modified by manganese species to obtain Mn/MgAl-LDH. The obtained modified MgAl-LDHs were characterized by inductively coupled plasma (ICP), X-ray powder diffraction (XRD), Fourier-transform infrared spectroscopy (FTIR), scanning electron microscopy-energy-dispersive X-ray analysis and X-ray photoelectron spectroscopy (XPS), measurements. The potency of the obtained material was then investigated towards the decomposition and removal of hydrazine. All experimental factors controlling the hydrazine removal and the mechanism type of its removal were investigated.

2. Materials and methods

2.1. Chemicals

Magnesium nitrate ($Mg(NO_3)_2·6H_2O$), aluminum nitrate ($Al(NO_3)_3·9H_2O$), sodium hydroxide (NaOH), sodium carbonate (Na_2CO_3), manganese sulfate ($MnSO_4·H_2O$), hydrazine (N_2H_4) and hydrochloric acid (HCl) were A.R. grade and used as received without any further treatment. A hydrazine stock solution (1,000 mg L^{-1}) was prepared and used for obtaining the desired concentration range of hydrazine solutions by dilution with de-ionized water. The solutions pH was tuned using HCl (0.1 mol L^{-1}) and NaOH (0.1 mol L^{-1}) solutions.

2.2. Apparatus

The inductively coupled plasma mass spectrometer (7800 ICP-MS, Agilent Technologies, USA) was used for the determination of Al, Mg and Mn. FTIR spectra within the range 400–4,000 cm^{-1} of samples were obtained using a Fourier-infrared spectrometer (FTIR: Nicolet 6700, Thermo Scientific, USA). Powder XRD patterns were performed on an advanced X-ray diffractometer (Bruker D8 Advance, Germany), using Ni-filtered Cu-Kα line as a radiation source (λ = 1.54056 Å). The surface morphology was investigated by scanning electron microscopy (SEM) (Quanta 250 FEG, The Netherlands). XPS analysis was performed using a Thermo Scientific ESCALAB 250 (USA) with a monochromatic Al Kα source. Peak shift due to charge compensation was corrected using the binding energy of C1s peak (C–C) = 284.5 eV. All peaks were fitted using the SMART background option. A UV-Visible spectrophotometer Agilent Cary 60 UV-Vis Spectrophotometer (Agilent Technologies, USA) was used for the determination of hydrazine concentrations before and after decomposition.

2.3. Synthesis of MgAl-LDH

The MgAl-LDH was prepared using a conventional coprecipitation method previously described [35] with a

slight modification. Typically, $Mg(NO_3)_2 \cdot 6H_2O$ (0.36 mol) and $Al(NO_3)_3 \cdot 9H_2O$ (0.09 mol) were firstly dissolved in distilled water. Then a solution containing NaOH (0.72 mol) and Na_2CO_3 (0.36 mol) in distilled water was added to the first solution dropwise, with vigorous stirring at room temperature. The suspension was then aged at room temperature for 24 h. The obtained precipitate was filtered and washed with excess distilled water. It was then dried at 80°C in an oven for 24 h to obtain MgAl-LDH.

2.4. Synthesis of Mn/MgAl-LDH

The Mn/MgAl-LDH was synthesized by a blending of 2.0 g of MgAl-LDH with a 35 mL aqueous solution of 0.1 M $MnSO_4 \cdot H_2O$. The mixture was heated at about 90°C for 2 h with stirring at 120 rpm. The obtained precipitate was separated by filtration, rinsed with distilled water several times followed by drying at 80°C.

2.5. Decomposition and removal of hydrazine

The assessment of hydrazine removal and decomposition was carried out using the batch technique. All experiments were performed in 150 mL conical flask with 50 mL working volume of hydrazine solution at the requested amount of the MgAl-LDH or Mn/MgAl-LDH. The experimental factors were studied at requested temperatures and time at a stirring rate of 120 rpm. The hydrazine concentrations were determined using *p*-dimethylamino-benzaldehyde reagent [36]. The removal and decomposition percent (%) at a time (*t*, min) were calculated using Eq. (3):

$$\text{Removal } (\%) = \left[\frac{C_0 - C}{C_0} \right] \times 100 \tag{3}$$

where C_0 (mg L^{-1}) was the initial hydrazine concentration, C (mg L^{-1}) was the remaining concentration of the hydrazine.

3. Results and discussion

3.1. Characterization of Mn/MgAl-LDH

Table 1 shows the ICP results of the MgAl-LDH and the Mn/MgAl-LDH. The MgAl ratio of MgAl-LDH was 3.591 which changed to 3.31 in the case of the Mn substituted MgAl-LDH. The percentage of magnesium content

Table 1
ICP analysis and molar ratio of MgAl-LDH and Mn/MgAl-LDH samples

Sample	wt.%				Color
	Mg%	Al%	Mn%	(MgAl)	
MgAl-LDH	23.81	6.63	0	3.591	
Mn/MgAl-LDH	20.45	6.18	6.976	3.31	

slightly decreased in Mn/MgAl-LDH comparing to pure MgAl-LDH. Moreover, the white color of MgAl-LDH turned to dark brown for the Mn/MgAl-LDH probably due to the formation of some manganese species [37,38]. The preliminary results imply a perception about the replacement of magnesium by manganese in the obtained LDH and/or formation of new phases.

The XRD patterns of pure MgAl-LDH and the Mn/MgAl-LDH are illustrated in Fig. 1. The pattern of pure MgAl-LDH displays all characteristic diffraction peaks at the (003), (006), (009), (015), (018), (110) and (113) corresponding to hydrotalcite-like compounds [39,40]. The calculated basal spacing, d_{003} was 7.9 Å indicating the existence of the intercalated CO_3^{2-} species and water molecules in the interlayer spaces [39]. The diffraction pattern of Mn/MgAl-LDH shows all characteristic peaks of pure MgAl-LDH as well as two new phases corresponding to $MnCO_3$ and Mn_3O_4. The observed diffraction lines at $2\theta = 24.3°, 31.4°, 37.5°, 41.5°$ and $51.7°$ are indexed to $MnCO_3$ (Rhodochrosite, JCPDS card no: 44-1472) [41,42]. The four diffraction peaks around $2\theta = 18.0°, 28.9°, 32.5°$ and $36.0°$ correspond to Mn_3O_4 [38,43].

The obtained results may reveal a possible isomorphism substitution of metal ions (Mg^{2+}/Al^{3+}) by manganese due to the diversity of ionic radii ($Mn^{2+} = 0.83$; $Mg^{2+} = 0.72$ Å; $Al = 0.53$ Å) [31]. Meanwhile, in our experimental conditions, we believe that some of Mn^{2+} may be facilely oxidized to higher oxidation state Mn^{3+}. Basically, the favorable converting of Mn^{2+} to Mn^{3+} in basic medium may be attributed to the low redox potential $\{E^0[Mn(OH)_3/Mn(OH)_2] = 0.1 \text{ V}\}$ [31,44]. Hence, the obtained dark brown of the Mn/MgAl-LDH can be attributed to the substantial converting of $Mn(OH)_2$ to husmannite (Mn_3O_4) in presence of air[38].

Fig. 2 presents FTIR of pure MgAl-LDH and Mn/MgAl-LDH before and after the decomposition of hydrazine. Broadband at about 3,470 cm^{-1} is mainly assigned to the stretching vibration of O–H groups. An observed band at 1,650 cm^{-1} is attributed to the bending vibration of H_2O intercalated between the layers. The absorption band at around 1,376 cm^{-1} in the pure MgAl-LDH spectrum is indexed to the stretching vibration of CO_3^{2-} in the interlayer [45]. The intense band at about 650 cm^{-1} may be related to metal-oxygen bonds in the LDH lattice [46]. The FTIR spectra of the Mn/MgAl-LDH before and after hydrazine decomposition show strong bands at 1,450 cm^{-1} corresponding to the anti-symmetric stretching mode of CO_3^{2-} [47]. The spectra of both samples also display a weak peak at 1,797 cm^{-1} assigning to the band related to the combination of CO_3^{2-} anions and Mn^{2+} ion [48]. In addition, the FTIR spectrum of Mn/MgAl-LDH after hydrazine decomposition does not reveal the characteristic peak corresponding to N_2H_2 at 1,614 cm^{-1} [49]. This finding indicates that the process of hydrazine removal is mainly based on catalytic decomposition rather than adsorption.

Morphology of pure LDH and Mn/MgAl-LDH before and after hydrazine decomposition is shown in Fig. 3. The SEM images of all samples display a plate-like morphology of LDHs that look in the form of rectangular shapes [50]. The SEM images show also separate and aggregated spherical shape particles confirming the formation of $MnCO_3$.

The surface elemental compositions of Mn/MgAl-LDH were verified by XPS. In Fig. 4a, all peaks of Mn 2p, O1s,
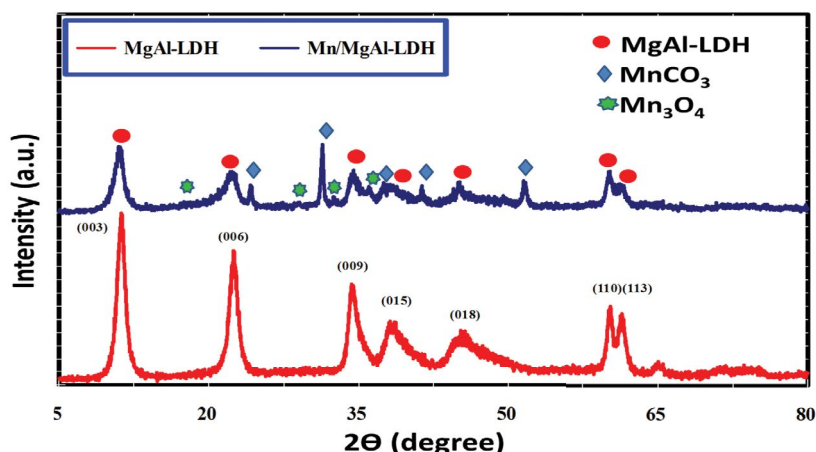
Fig. 1. XRD patterns of pure MgAl-LDH and Mn/MgAl-LDH.
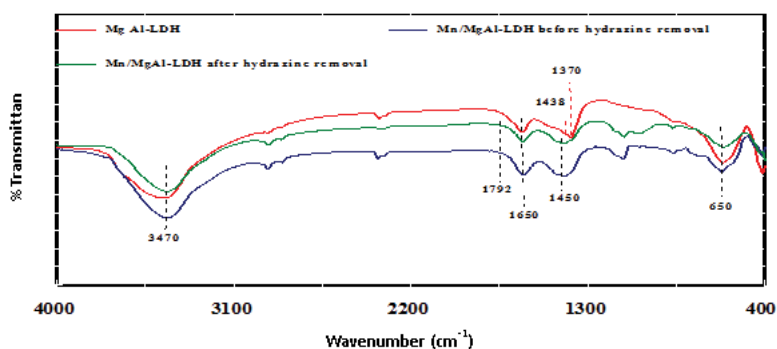
Fig. 2. FTIR spectra of pure MgAl-LDH and Mn/MgAl-LDH after and before hydrazine decomposition.

C1s, Al 2p, Mg 1s, and S 2p are shown in the wide scan XPS spectra indicating the presence of Mn, O, C, Al, Mg and S elements on the surface of the sample.

The deconvoluted XPS peaks of O1s for Mn/MgAl-LDH (Fig. 4b) show three peaks; the first peak at 529.8 eV referrers to the lattice oxygen in $MnCO_3$ and/or Mn_3O_4, while peaks at 531.8 and 533.6 eV are assigned to surface-adsorbed oxygen (like O_2^{-2}, O^-, etc.) and water at the surface[51–53]. Meanwhile, the quantitative analysis shows the high atomic percentage of oxygen (58%) implying its abundance on the surface.

The high resolution C1s spectrum (Fig. 4c) displays three fitted peaks, 284.9 eV for C–C (adventitious carbon), 286.8 eV for C–O and 289.8 eV for CO_3^{2-} anion in $MnCO_3$ [51,54].

The XPS for the Mn 2p emission line (Fig. 4d) shows a spin-orbit doublet with Mn $2p_{3/2}$ at 641.1 eV and Mn $2p_{1/2}$ at 653.6 eV. The peak fitting deconvolution Mn $2p_{3/2}$ exhibits two peaks at 641.1 and 642.4 eV assigning to Mn^{2+} and Mn^{3+}, respectively [55]. The shake-up peak located at 646.7 eV was also assigned to Mn^{2+} species These results are in agreement with XRD and certainly prove that the Mn^{2+} and Mn^{3+} are loaded on the surface as Mn_3O_4 [56]. In the same context, the observed *S* in the wide scan XPS spectra can be attributed to the presence of a little residual amount of SO_4^{2-}.

3.2. Performance of Mn/MgAl-LDH towards the hydrazine decomposition

The decomposition of hydrazine was investigated using Mn/MgAl-LDH sample in a batch-type process. The experimental factors related to the hydrazine decomposition process like pH, reaction time, an initial hydrazine concentration and reaction temperature were investigated.

3.2.1. Influence of pH

Fig. 5a displays the pH influence on the decomposition of hydrazine over the pH range from 3 to 10 for an initial hydrazine 10 mg L^{-1}, stirring time 60 min and an Mn/MgAl-LDH dosage of 100 mg. It can be seen that the removal and decomposition ratio of hydrazine increases with an increase in solution pH from 3.0 to 8.0 and thereafter slightly decreases for pH greater than 8.0. The decomposition ratio is found to be 65% at pH 3 and reaches a maximum value of 88% at pH 8. The decomposition of hydrazine is mainly attributed to the already presence of the Mn^{3+} ions and Mn_3O_4 on the surface. Basically, Mn(III) is a strong oxidizing reagent involving one-electron transfer. Moreover, the composition of Mn_3O_4 is influenced by the pH value. It can be dissolved to form Mn^{2+} rather than Mn^{3+} at a low acidic
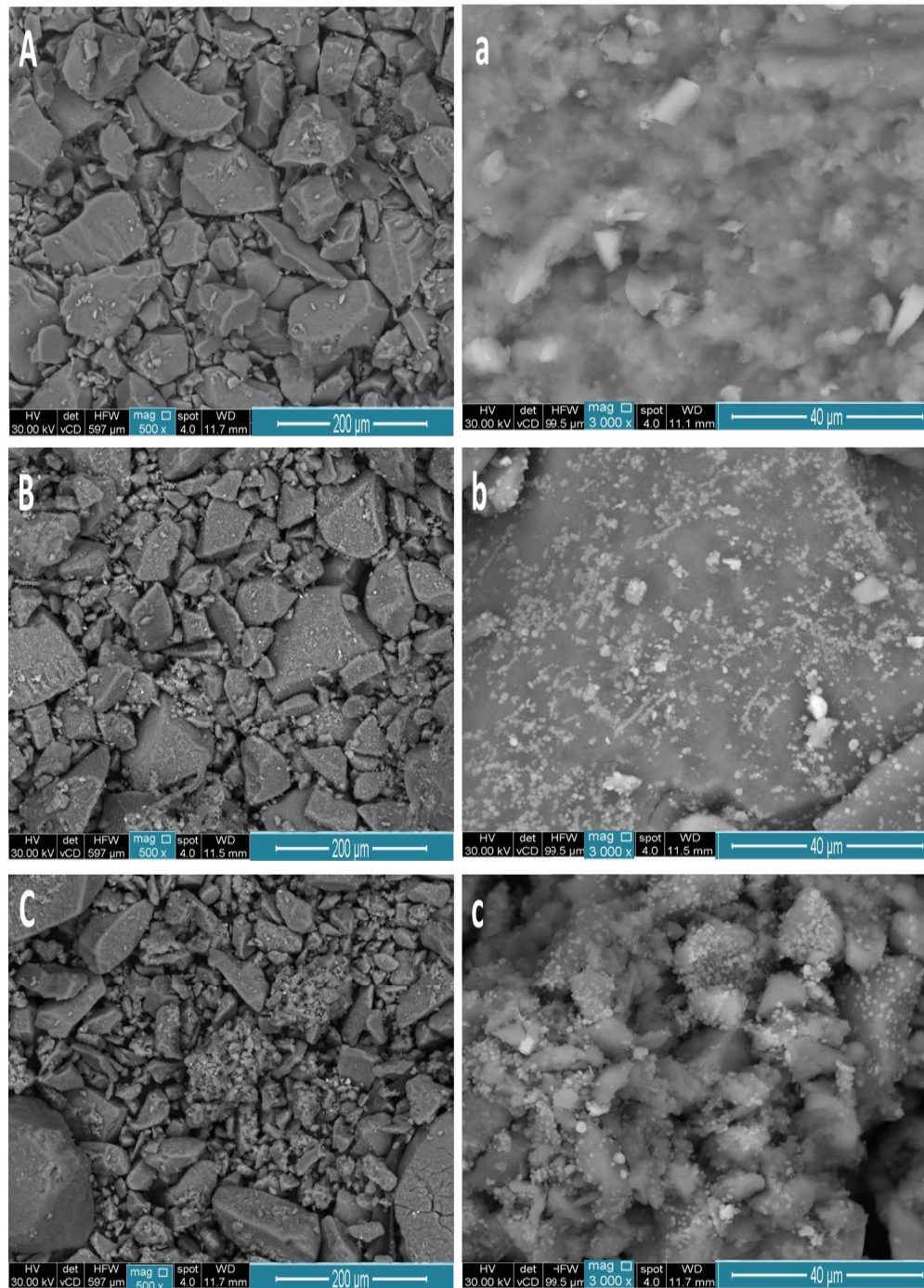
Fig. 3. SEM of pure MgAl-LDH (A,a), and Mn/MgAl-LDH before (B,b), and after hydrazine decomposition (C,c) at different magnifications; (A–C) 500× and (a–c) 3,000×.

medium [53]. Hence, the enhanced decomposition of hydrazine at basic pH can be referred to the existence of more Mn^{3+} [31,44,53] which assists the decomposition of hydrazine.

3.2.2. Influence of time

The decomposition of hydrazine vs. time was investigated by varying time in the range from 5 to 90 min for an initial hydrazine concentration of 10 mg L^{-1} and pH 8.0 at 20°C (293 K). In Fig. 5b, the decomposition of hydrazine gradually increases with time to reach 100% degradation at 90 min. Meanwhile, at the same experimental conditions, the pure MgAl-LDH sample shows about 14% of hydrazine decomposition and removal in comparison with the Mn-substituted MgAl-LDH. This result confirms the ability of modified MgAl-LDH by Mn for hydrazine decomposition.
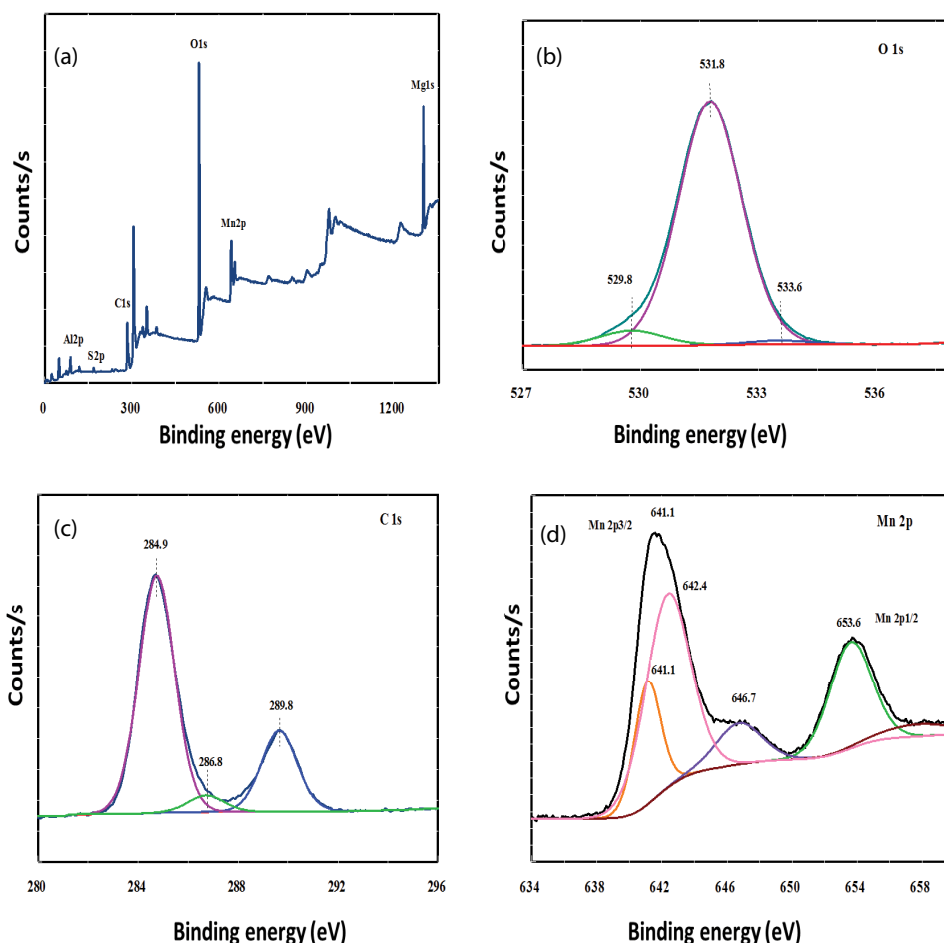
Fig. 4. XPS spectra of Mn/MgAl-LDH: survey spectrum (a), O1s (b), C1s (c), and Mn 2p (d).

3.2.3. Influence of the initial hydrazine concentration

Fig. 5c depicts the decomposition ratio of hydrazine vs. the initial hydrazine concentration ranging from 5 to 150 mg L^{-1} at the solution pH of 8.0 with Mn/MgAl-LDH dosage of 100 mg in 50 mL at 20°C (293 K). The hydrazine decomposition is totally accomplished (100% removal) at hydrazine concentrations of 5, 10 and 15 mg L^{-1}. The decomposition ratio then decreases from 92.7% to 35.6% as the initial hydrazine concentration increases from 25 to 150 mg L^{-1}. The higher decomposition ratio at lower hydrazine concentrations can be assigned to the available many active sites that have the ability for the decomposition of the particular amount of hydrazine.

3.2.4. Influence of reaction temperature

Fig. 5d shows the influence of temperature on the decomposition of hydrazine at 293, 303 and 318 K. In general, the decomposition ratio of hydrazine increases with increasing the temperature from 293 to 318 K. Moreover, with increasing temperature in the same order, the time required for complete hydrazine decomposition reduces from 90 to 60 and finally becomes 45 min.

3.3. Kinetic studies

The decomposition kinetics of hydrazine was investigated by applying the linear forms of the zero (Eq. (4)), first (Eq. (5)) and second (Eq. (6)) order rate law.

$$C_0 - C = k_0 t \tag{4}$$

$$\ln\left(\frac{C_0}{C}\right) = k_1 t \tag{5}$$

$$\frac{1}{C} - \frac{1}{C_0} = k_2 t \tag{6}$$

where C_0 and C represent the concentrations of hydrazine at time zero and t, min, respectively. Values of k_0, k_1 and k_2 show the rates constant of zero, first, and second-order kinetic models, respectively. The fitted experimental data to the proposed models are shown in Fig. 6. Obviously, the experimental results are incompatible with both zero and second-order models (Figs. 6a and c) which display correlation coefficients (R^2) of 0.923 and 0.841, respectively. While
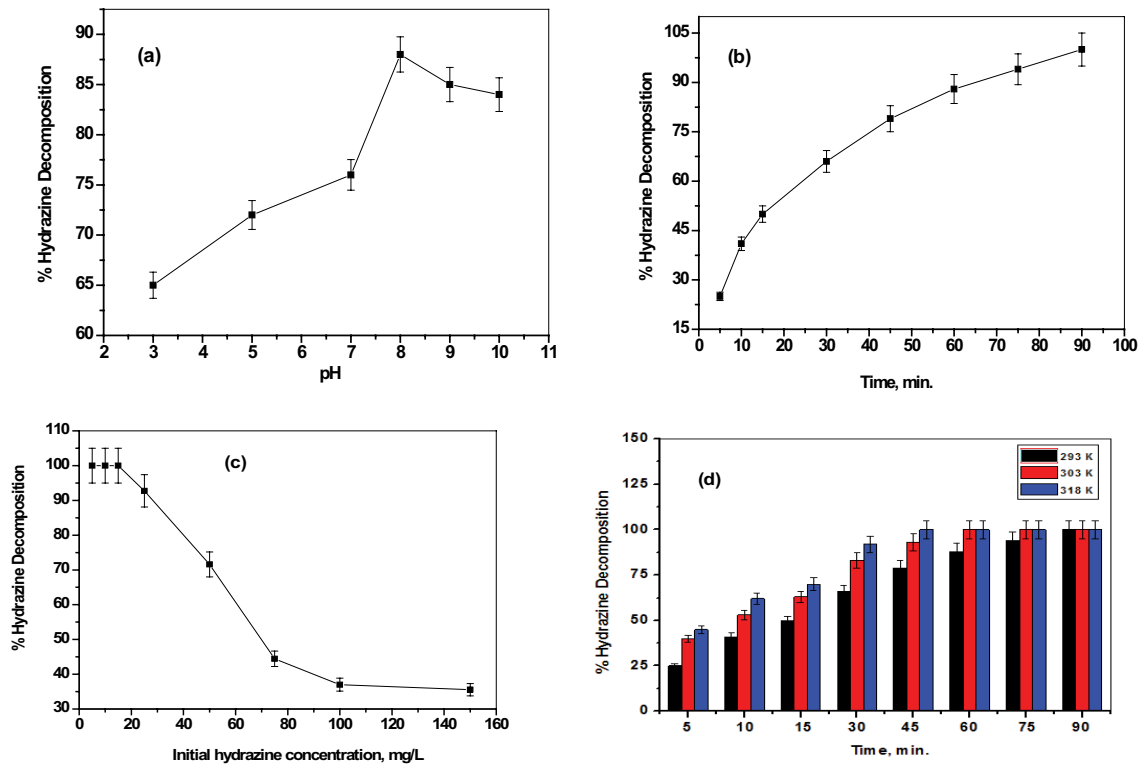
Fig. 5. Effect of pH (a), reaction time (b), initial concentration of hydrazine (c), and reaction temperature (d) on hydrazine decomposition by Mn/MgAl-LDH.
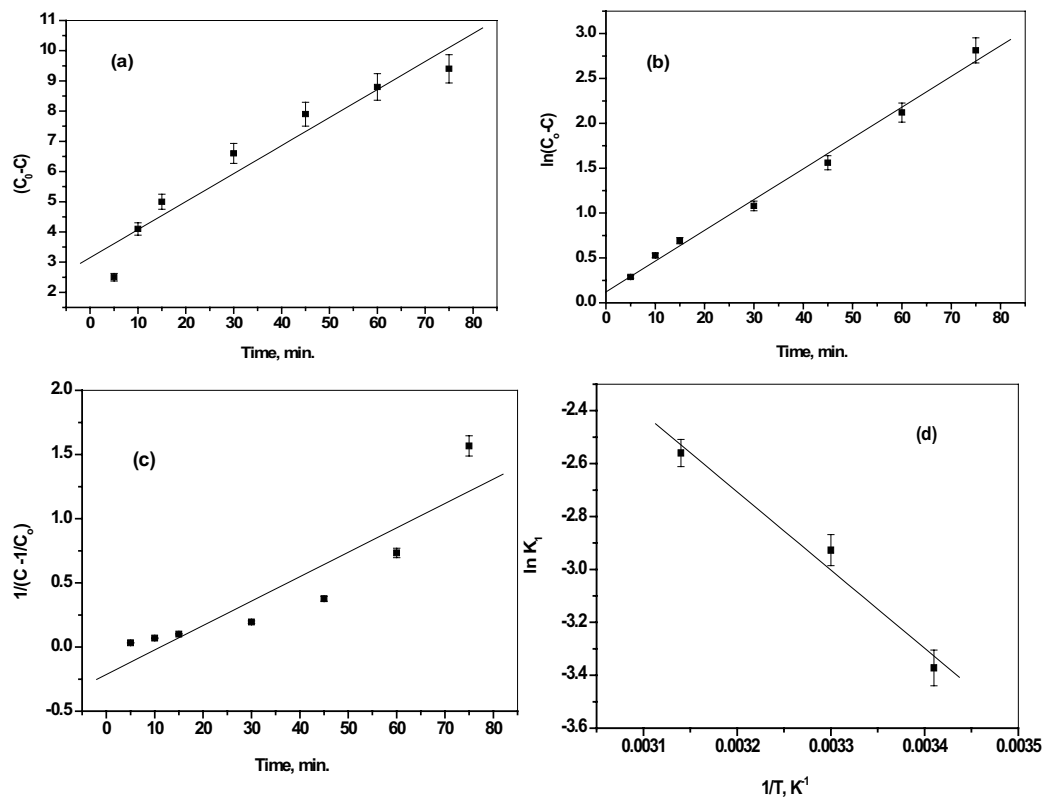
Fig. 6. Kinetic models for the decomposition of hydrazine over Mn/MgAl-LDH: zero-order (a), first-order (b), and second-order (c), dependence of hydrazine decomposition rate on the $1/T$ (d).
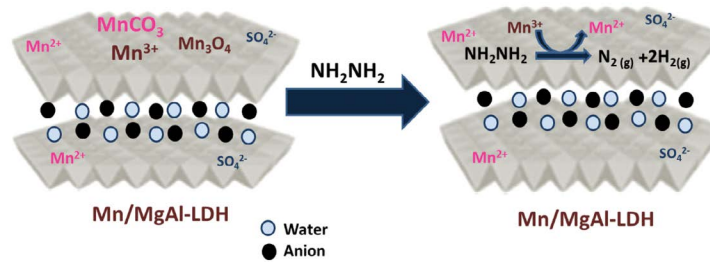
Fig. 7. Mechanism of hydrazine decomposition on Mn/MgAl-LDH.

the derived data points of the first-order model (Fig. 6b) exhibits a well straight line with a higher correlation coefficient (R^2) of 0.992. The obtained k_1 value from the slope of the straight line is 0.034 min^{-1}. The activation energy (E_a) of the hydrazine decomposition can be obtained from the slope of plotting ln$k$ against 1/T (Arrhenius Eq. (7) and Fig. 6d).

$$\ln k = \ln A - \frac{E_a}{RT} \tag{7}$$

where k is the rate constant, R is the universal gas constant (8.314 J mol^{-1} K^{-1}) and A is the pre-exponential factor. The E_a value is found to be 24.841 kJ mol^{-1}.

3.4. Possible mechanism of hydrazine decomposition on Mn/MgAl-LDH

Due to the characteristic nature of MgAl-LDH and the experimental conditions, some metal ions (Mg^{2+}/Al^{3+}) were undergone isomorphous substitution by Mn^{2+} which could be facilely oxidized to higher oxidation state Mn^{3+}. The detailed XPS and XRD results proved that the Mn/MgAl-LDH contained Mn^{2+}, Mn^{3+} ions and Mn_3O_4 on the surface. Meanwhile, the FTIR spectroscopy indicated that the process of hydrazine removal was mainly based on catalytic decomposition than adsorption. Basically, the direct complete decomposition of hydrazine on the surface at a lower

Table 2
Comparison of the hydrazine decomposition and removal by Mn/MgAl-LDH with some other studies

Material	Method	Conditions	Results	Reference
Tremelliform Co0.85Se nanosheets	Catalytic decomposition	50 mg Co0.85Se catalyst; (N_2H_4) = 2 × 10^{-3} M, pH = 11.3; temperature = 298 K, time = 50 min	Hydrazine conversion rate up to 95% after 50 min	[58]
Sargassum ilicifolium	Biosorption	Biosorbent dose = 0.1 g L^{-1}; (N_2H_4) = 135 mg L^{-1}; pH = 7.5, temperature = 298 K; time = 90 min	Biosorption capacity, (q_m = 189.1 mg g^{-1})	[13]
Coal ash	Ultrasonic irradiation and decomposition	Coal ash dose = 2 g L^{-1}; (N_2H_4) = 3.2 mg L^{-1}; pH = 8; temperature = 293 K; time = 60 min	Removal capacity, (q_m = 0.16 mg g^{-1})	[11]
Coal ash	Ultrasonic irradiation, decomposition and adsorption	Coal ash dose = 2 g L^{-1}; (N_2H_4) = 3.2 mg L^{-1}; pH = 8, temperature = 293 K; time = 60 min	Removal capacity, (q_m = 0.16 mg g^{-1})	[12]
DQ-COF/Ni composite	Adsorption	Adsorbent dose = 10 mg; (N_2H_4) = 100 mg L^{-1}; pH = 7; temperature = 298 K; time = 90 min	Removal capacity, (q_m = 1,108 mg g^{-1})	[16]
Mn/MgAl-LDH	Decomposition and removal	Mn/MgAl-LDH dose = 100 mg; (N_2H_4) = 5, 10 and 15 mg L^{-1}; pH = 8; temperature = 293 K; time = 90 min	100% removal	[This work]
		Mn/MgAl-LDH dose = 100 mg; (N_2H_4) = 25–150 mg L^{-1}; pH = 8; temperature = 293 K; time = 90 min	92.7%–35.6% removal	
		Mn/MgAl-LDH dose = 100mg; (N_2H_4) = 10 mg L^{-1}; pH = 8; temperature = 303; time = 60 min	100% removal	
		Mn/MgAl-LDH dose = 100mg; (N_2H_4) = 10 mg L^{-1}; pH = 8; temperature = 318 K; time = 45 min	100% removal	

temperature can follow Eq. (1) [4,57]. The superiority of Mn/MgAl-LDH for hydrazine decomposition than MgAl-LDH was mainly attributed to the existence of manganese species. Hence, the proposed mechanism of the hydrazine decomposition by Mn/MgAl-LDH can be illustrated as shown in Fig. 7. The coexistence of both Mn^{2+} and Mn^{3+} ions as well as Mn_3O_4 is essential for the oxidation of hydrazine and decomposition. When hydrazine molecules get in contact with the surface of Mn/MgAl-LDH, they are oxidized by Mn^{3+} ions on the surface of MgAl-LDH and that present in Mn_3O_4. Thence, hydrazine molecules are decomposed to N_2 and H_2.

4. Conclusions

The Mn/MgAl-LDH sample has been synthesized by a facile approach using manganese sulfate. The obtained sample exhibited a good effect on the decomposition and removal of hydrazine. The results showed that the hydrazine decomposition and removal is pH, time, initial hydrazine concentration. At pH 8 and time of 90 min, the hydrazine decomposition was 100% at lower concentrations (5, 10 and 15 mg L^{-1}), while the decomposition ratio decreased from 92.7% to 35.6% for the increased hydrazine concentration from 25 to 150 mg L^{-1}. The decomposition of hydrazine was greatly influenced by temperature, in which the decomposition ratio increased with increasing the temperature from 293 to 318 K. Moreover, the time required for complete hydrazine decomposition reduced from 90 to 60 and finally became 45 min with the same increasing order of temperature. The catalytic decomposition of hydrazine was best followed by the first-order rate law with calculated E_a of 24.841 kJ mol^{-1}. The superior performance of Mn/MgAl-LDH was recognized by comparing the efficacy of pure MgAl-LDH sample for hydrazine decomposition, which showed 14% of hydrazine decomposition and removal. Here, due to the characteristic nature of MgAl-LDH and the experimental conditions, an isomorphism substitution of metal ions (Mg^{2+}/Al^{3+}) by manganese certainly occurred and some of Mn^{2+} could be facilely oxidized to higher oxidation state Mn^{3+}. Consequently, the considerable enhancing of hydrazine decomposition by Mn/MgAl-LDH was mainly due to the existence of Mn^{3+} ions Mn_3O_4 on the surface. The obtained results were reviewed and compared with other performed studies (Table 2). The results show the ability and effectiveness of the current material for hydrazine removal compared with some instrumental techniques. Moreover, the simplicity of the Mn/MgAl-LDH preparation as well as the method of hydrazine removal (patch technique) give the study a distinct advantage for application and can be extended for further studies concerning hydrazine.

Acknowledgment

References

[1] P. Wuamprakhon, A. Krittayavathananon, N. Ma, N. Phattharasupakun, T. Maihom, J. Limtrakul, M. Sawangphruk, Layered manganese oxide nanosheets coated on N-doped graphene aerogel for hydrazine detection: reaction mechanism investigated by in situ electrochemical X-ray absorption spectroscopy, J. Electroanal. Chem., 808 (2018) 124–132.

[2] H. Nakui, K. Okitsu, Y. Maeda, R. Nishimur, Hydrazine degradation by ultrasonic irradiation, J. Hazard. Mater., 146 (2007) 636–639.

[3] M.Y. Wang, W. Wang, M. Ji, X.L. Cheng, Adsorption of phenol and hydrazine upon pristine and X-decorated (X = Sc, Ti, Cr and Mn) MoS$_2$ monolayer, Appl. Surf. Sci., 439 (2018) 350–363.

[4] K.V. Manukyan, A. Cross, S. Rouvimov, J. Miller, A.S. Mukasyan, E.E. Wolf, Low temperature decomposition of hydrous hydrazine over FeNi/Cu Nanoparticles, Appl. Catal. A, 476 (2014) 47–53.

[5] D.W. Johnson, M.W. Roberts, Adsorption of hydrazine and ammonia on aluminum, J. Electron Spectrosc. Relat. Phenom., 19 (1980)186–195.

[6] R. Dopheide, L. Schrijter, H. Zacharias, Adsorption and decomposition of hydrazine on Pd(100), Surf. Sci., 257 (1991) 86–96.

[7] I.J. Jang, H.S. Shin, N.R. Shin, S.H. Kim, S.K. Kim, M.J. Yu, S.J. Cho, Macroporous–mesoporous alumina supported iridium catalyst for hydrazine decomposition, Catal. Today, 185 (2012) 198–204.

[8] S.J. Cho, J. Lee, Y.S. Lee, D.P. Kim, Characterization of Iridium catalyst for decomposition of hydrazine hydrate for hydrogen generation, Catal. Lett., 109 (2006) 181–186.

[9] J. Sun, B.L. Liang, Y.Q. Huang, X.D. Wang, Synthesis of nanostructured tungsten carbonitride (WN$_x$C$_y$) by carbothermal ammonia reduction on activated carbon and its application in hydrazine decomposition, Catal. Today, 274 (2016) 123–128.

[10] K. Sunitha, P. Nikhitha, S.V. Satyanarayana, S. Sridhar, Recovery of hydrazine and glycerol from aqueous solutions by membrane separation techniques, Sep. Sci. Technol., 46 (2011) 2418–2426.

[11] H. Nakui, K. Okitsu, Y. Maeda, R. Nishimura, Effect of coal ash on hydrazine degradation under stirring and ultrasonic irradiation conditions, Ultrason. Sonochem., 15 (2008) 472–477.

[12] H. Nakui, K. Okitsu, Y. Maeda, R. Nishimura, Sonochemical decomposition of hydrazine in water: effects of coal ash and pH on the decomposition and adsorption behavior, Chemosphere, 76 (2009) 716–720.

[13] R. Tabaraki, A. Nateghi, Application of taguchi L16 orthogonal array design to optimize hydrazine biosorption by Sargassum ilicifolium, Environ. Prog. Sustainable Energy, 35 (2016) 1450–1457.

[14] A.L. Cazetta, T. Zhang, T.L. Silva, V.C. Almeida, Bone char-derived metal-free N- and S-co-doped nanoporous carbon and its efficient electrocatalytic activity for hydrazine oxidation, Appl. Catal., B, 225 (2018) 30–39.

[15] K. Yang, K.K. Yang, S.L. Zhang, Y. Luo, Q. Yao, Z.-H. Lu, Complete dehydrogenation of hydrazine borane and hydrazine catalyzed by MIL-101 supported NiFePd nanoparticles, J. Alloys Compd., 732 (2018) 363–371.

[16] C.Y. Liang, H.M. Lin, Q. Wang, E. Shi, S.H. Zhou, F. Zhang, F. Qu, G.S. Zhu, A redox-active covalent organic framework for the efficient detection and removal of hydrazine, J. Hazard. Mater., 381 (2020) 120983.

[17] F. Cavani, F. Trifiro, A. Vaccari, Hydrotalcite-type anionic clays: preparation, properties and applications, Catal. Today, 11 (1991) 173–301.

[18] N. Gerds, V. Katiyar, C.B. Koch, J. Risbo, D. Plackett, H.C.B. Hansen, Synthesis and characterization of laurate-intercalated MgAl-layered double hydroxide prepared by co-precipitation, Appl. Clay Sci., 65–66 (2012) 143–151.

[19] M. Dinari, M.M. Momeni, Y. Ghayeb, Photodegradation of organic dye by ZnCrLa-layered double hydroxide as visible-light photocatalysts, J. Mater. Sci.-Mater. Electron, 27 (2016) 9861–9869.

[20] M. Dinari, M.M. Momeni, Z. Bozorgmehr, S. Karimi, Bismuth-containing layered double hydroxide as a novel efficient photocatalyst for degradation of methylene blue under visible light, J. Iran. Chem. Soc., 14 (2017) 695–701.

[21] M. Dinari, A. Haghighi, P. Asadi, Facile synthesis of ZnAl-EDTA layered double hydroxide/poly(vinyl alcohol) nanocomposites as an efficient adsorbent of Cd(II) ions from the aqueous solution, Appl. Clay Sci., 170 (2019) 21–28.

[22] O. Rahmanian, S. Amini, M. Dinari, Preparation of zinc/iron layered double hydroxide intercalated by citrate anion for capturing lead(II) from aqueous solution, J. Mol. Liq., 256 (2018) 9–15.

[23] O. Rahmanian, M. Dinari, M.K. Abdolmaleki, Carbon quantum dots/layered double hydroxide hybrid for fast and efficient decontamination of Cd(II): the adsorption kinetics and isotherms, Appl. Surf. Sci., 428 (2018) 272–279.

[24] M. Dinari, S. Neamati, Surface modified layered double hydroxide/polyaniline nanocomposites: synthesis, characterization and Pb^{2+} removal, Colloids Surf., A, 589 (2020) 124438.

[25] M. Dinari, M.A. Shirani, M.H. Maleki, R. Tabatabaeian, Green cross-linked bionanocomposite of magnetic layered double hydroxide/guar gum polymer as an efficient adsorbent of Cr(VI) from aqueous solution, Carbohydr. Polym., 236 (2020) 116070.

[26] W. Chen, L. Feng, B.J. Qu, In situ synthesis of poly(methyl methacrylate)/MgAl-layered double hydroxide nanocomposite with high transparency and enhanced thermal properties, Solid State Commun.,130 (2004) 259–263.

[27] X. Yuan, Y.F. Wang, J. Wang, C. Zhou, Q. Tang, X.B. Rao, Calcined graphene/MgAl-layered double hydroxides for enhanced Cr(VI) removal, Chem. Eng. J., 221 (2013) 204–213.

[28] S. Mallakpour, M. Dinari, M. Hatami, Novel nanocomposites of poly(vinyl alcohol) and MgAl-layered double hydroxide intercalated with diacid *N*-tetrabromophthaloyl-aspartic, J. Therm. Anal. Calorim., 120 (2015) 1293–1302.

[29] T. Kameda, H. Takeuchi, T. Yoshioka, Kinetics of uptake of Cu^{2+} and Cd^{2+} by MgAl-layered double hydroxides intercalated with citrate, malate, and tartrate, Colloids Surf., A, 355 (2010) 172–177.

[30] X.F. Zhang, L.Y. Ji, J. Wang, R. Li, Q. Liu, M.L. Zhang, L.H. Liu, Removal of uranium(VI) from aqueous solutions by magnetic MgAl-layered double hydroxide intercalated with citrate: kinetic and thermodynamic investigation, Colloids Surf., A, 414 (2010) 220–227.

[31] S. Velu, N. Shah, T.M. Jyothi, S. Sivasanker, Effect of manganese substitution on the physicochemical properties and catalytic toluene oxidation activities of MgAl-layered double hydroxides, Microporous Mesoporous Mater., 33 (1999) 61–75.

[32] J. Arulraj, M. Rajamathi, Preparation of anionic clay–birnessite manganese oxide composites by interlayer oxidation of oxalate ions by permanganate, J. Solid State Chem., 198 (2013) 303–307.

[33] M. Raciulete, G. Layrac, F. Papa, C. Negrila, D. Tichit, I.C. Marcu, Influence of Mn content on the catalytic properties of Cu-(Mn)-Zn-Mg-Al mixed oxides derived from LDH precursors in the total oxidation of methane, Catal. Today, 306 (2018) 276–286.

[34] X.C. Zhu, H. Liu, D. Skala, Manganese carbonate-zinc glycerolate, synthesis, characterization and application as catalyst for transesterification of soybean oil, Chem. Ind. Chem. Eng. Q., 22 (2016) 431–443.

[35] J. Chen, L. Lv, J. He, L. Xv, Kinetic and equilibrium study on uptake of iodide ion by calcined layered double hydroxides, Desal. Water Treat., 42 (2012) 279–288.

[36] C. Gojon, B. Dureault, Spectrophotometric study of the reaction between hydrazine and *p*. dimethylaminobenzaldhyde, J. Nucl. Sci. Technol., 33 (1996) 731–735.

[37] K.U. Madhu, C.K. Mahadevan, Dielectric studies of manganese carbonate nanocrystals, Int. J. Eng. Res. Appl., 3 (2013) 2264–2267.

[38] S. Said, M. Raid, S. Mikhail, Preparation of different manganese oxide structures via controlling the concentration and the type of the alkaline media, Asian J. Nanosci. Mater., 2 (2019) 286–300.

[39] U. Costantino, F. Marmottini, R. Nocchetti, R. Vivani, New synthetic routes to hydrotalcite-like compounds-characterization and properties of the obtained materials, Eur. J. Inorg. Chem., 10 (1988) 1439–1446.

[40] K. Yang, L.-g. Yan, Y.-m. Yang, S.-j. Yu, R.-r. Shan, H.-q. Yu, B.-c. Zhu, B. Du, Adsorptive removal of phosphate by MgAl

[41] and Zn-Al-layered double hydroxides: kinetics, isotherms and mechanisms, Sep. Purif. Technol., 124 (2014) 36–42.

[41] H.H. Peng, L. Zhang, D.Y. Jiang, J. Chen, Facile synthesis of MnCO$_3$ nanoparticles on Ni foam for binder-free super capacitor electrodes, Int. J. Electrochem. Sci., 12 (2017) 5898–5909.

[42] S.C. Sekhar, G. Nagaraju, J.S. Yu, Ant-cave structured MnCO$_3$/Mn$_3$O$_4$ microcubes by biopolymer-assisted facile synthesis for high-performance pseudo capacitors, Appl. Surf. Sci., 435 (2018) 398–405.

[43] F.Y. Zeng, Y. Pan, Y. Yang, Q.L. Li, G.Y. Li, Z.H. Hou, G. Gu, Facile construction of Mn$_3$O$_4$-MnO$_2$ hetero-nanorods/graphene nanocomposite for highly sensitive electrochemical detection of hydrogen peroxide, Electrochim. Acta, 196 (2016) 587–596.

[44] B. Dong, W. Li, X.X. Huang, Z.H. Ali, T. Zhang, Z. Yang, Y.L. Hou, Fabrication of hierarchical hollow Mn doped Ni(OH)$_2$ nanostructures with enhanced catalytic activity towards electrochemical oxidation of methanol, Nano Energy, 55 (2019) 37–41.

[45] L. Yang, Z. Shahrivari, P.K.T. Liu, M. Sahimi, T.T. Tsotsis, Removal of trace levels of arsenic and selenium from aqueous solutions by calcined and uncalcined layered double hydroxides (LDH), Ind. Eng. Chem. Res., 44 (2005) 6804–6815.

[46] Y.W. Guo, Z.L. Zhu, Y.L. Qiu, J.F. Zhao, Adsorption of arsenate on Cu/Mg/Fe/La layered double hydroxide from aqueous solutions, J. Hazard. Mater., 239–240 (2012) 279–288.

[47] T. Wang, C. Li, C.Q. Wang, H. Wang, Biochar/MnAl-LDH composites for Cu(II) removal from aqueous solution, Colloids Surf., A, 538 (2018) 443–450.

[48] P.V. Vardhan, C. Jothilakshmi, U.K. Mudali, S. Devaraj, The effect of carbonate precursors on the capacitance properties of MnCO$_3$, Mater. Today: Proc., 4 (2017) 12407–12415.

[49] L. Ding, Y.Y. Shu, A.Q. Wang, M.Y. Zheng, L. Li, X.D. Wang, T. Zhang, Preparation and catalytic performances of ternary phosphides NiCoP for hydrazine decomposition, Appl. Catal., A, 385 (2010) 232–237.

[50] R. Chitrakar, S. Tezuka, A. Sonoda, K. Sakane, K. Ooi, T. Hirotsu, Synthesis and phosphate uptake behavior of Zr^{4+} incorporated MgAl-layered double hydroxides, J. Colloid Interface Sci., 313 (2007) 53–63.

[51] H. Chen, Z. Yan, X.Y. Liu, X.L. Guo, Y.X. Zhang, Z.H. Liu, Rational design of microsphere and microcube MnCO$_3$@MnO$_2$ heterostructures for super capacitor electrodes, J. Power Sources, 353 (2017) 202–209.

[52] J. Zhao, Y. Li, Z.Y. Xu, D. Wang, C.L. Ban, H.H. Zhang, Unique porous Mn$_2$O$_3$/C cube decorated by Co$_3$O$_4$ nanoparticle: low cost and high-performance electrode materials for asymmetric super capacitors, Electrochim. Acta, 289 (2018) 72–81.

[53] A. Gagrani, B. Ding, T. Wang, T. Tsuzuki, pH dependent catalytic redox properties of Mn$_3$O$_4$ nanoparticles, Mater. Chem. Phys., 231 (2019) 41–47.

[54] S. Ruan, C. Ma, J. Wang, W. Qiao, L. Ling, Facile synthesis of graphene wrapped porous MnCO$_3$ microspheres with enhanced surface capacitive effects for superior lithium storage, Chem. Eng. J., 367 (2019) 64–75.

[55] X.D. Wu, H. Yu, D. Weng, S. Liu, J. Fan, Synergistic effect between MnO and CeO$_2$ in the physical mixture: electronic interaction and NO oxidation activity, J. Rare Earths, 31 (2013) 1141–1147.

[56] Y. Li, T. Gai, L. Shao, H. Tang, R. Li, S.L. Yang, S.F. Wang, Q. Wu, Y.M. Ren, Synthesis of sandwich-like Mn$_3$O$_4$@reduced graphene oxide nano-composites via modified Hummers' method and its application as uranyl adsorbents, Heliyon, 5 (2019) e01972.

[57] S. Lee, C. Fan, T. Wu, S.L. Anderson, Hydrazine decomposition over Irn/Al$_2$O$_3$ model catalysts prepared by size-selected cluster deposition, J. Phys. Chem. B, 109 (2005) 381–388.

[58] C.-C. Liu, J.-M. Song, J.-F. Zhao, H.-J. Li, H.-S. Qian, H.-L. Niu, C.-J. Mao, S.-Y. Zhang, Y.-H. Shen, Facile synthesis of tremelliform Co0.85Se nanosheets: an efficient catalyst for the decomposition of hydrazine hydrate, Appl. Catal. B, 119–120 (2012) 139–145.